


RESEARCH

Open Access



Multiparametric grading of glaucoma severity by histopathology can enable post-mortem substratification of disease state

Chuanxi Xiang¹, VijayKrishna Raghunathan¹, Yubin Qiu¹, Manisha Mehta¹, John T. Demirs¹, Cynthia L. Grosskreutz¹, Christopher W. Wilson^{1*}  and Ganesh Prasanna^{1*}

Abstract

Neurodegeneration in glaucoma patients is clinically identified through longitudinal assessment of structure–function changes, including intraocular pressure, cup-to-disc ratios from fundus images, and optical coherence tomography imaging of the retinal nerve fiber layer. Use of human post-mortem ocular tissue for basic research is rising in the glaucoma field, yet there are challenges in assessing disease stage and severity, since tissue donations with informed consent are often unaccompanied by detailed pre-mortem clinical information. Further, the interpretation of disease severity based solely on anatomical and morphological assessments by histology can be affected by differences in death-to-preservation time and tissue processing. These are difficult confounders that cannot be easily controlled. As pathogenesis and molecular mechanisms can vary depending on the stage and severity of glaucoma, there is a need for the field to maximize use of donated tissue to better understand the molecular mechanisms of glaucoma and develop new therapeutic hypotheses. Further, there is a lack of consensus around the molecular RNA and protein markers that can be used to classify glaucoma severity. Here, we describe a multiparametric grading system that combines structural measurements of the retinal nerve fiber layer with linear regression and principal component analyses of molecular markers of retinal ganglion cells and glia (RBPMS, NEFL, IBA1 and GFAP) to stratify post-mortem glaucoma eyes by the severity of disease. Our findings show that a quantitative grading approach can stratify post-mortem glaucoma samples with minimal clinical histories into at least three severity groups and suggest that this type of approach may be useful for researchers aiming to maximize insights derived from eye bank donor tissue.

Keywords Glaucoma, Retinal nerve fiber layer, Pathology grading, Neurodegeneration, Histology, Multivariate analysis, Human donor tissues

Introduction

Glaucoma is an optic neuropathy that affects approximately 80 million people worldwide, with up to 10% of glaucoma patients progressing to complete blindness

[1–4]. It is characterized by progressive vision loss attributed to a loss of retinal ganglion cells (RGCs) and their axons, which form the optic nerve. Specifically, RGC loss accompanied by thinning of the retinal nerve fiber layer (RNFL) and cupping of the optic nerve head (ONH) are hallmarks of glaucomatous neuropathy [4, 5]. Several risk factors are associated with this disease; however, the only modifiable and treatable risk factor is elevated intraocular pressure (IOP). Current IOP-lowering treatments, either through pharmacological intervention (eye drops,

*Correspondence:

Christopher W. Wilson
chris.wilson@novartis.com

Ganesh Prasanna
ganesh.prasanna@novartis.com

¹ Ophthalmology, Novartis Biomedical Research, Cambridge, MA, USA



© Novartis BioMedical Research 2024. **Open Access** This article is licensed under a Creative Commons Attribution-NonCommercial-NoDerivatives 4.0 International License, which permits any non-commercial use, sharing, distribution and reproduction in any medium or format, as long as you give appropriate credit to the original author(s) and the source, provide a link to the Creative Commons licence, and indicate if you modified the licensed material. You do not have permission under this licence to share adapted material derived from this article or parts of it. The images or other third party material in this article are included in the article's Creative Commons licence, unless indicated otherwise in a credit line to the material. If material is not included in the article's Creative Commons licence and your intended use is not permitted by statutory regulation or exceeds the permitted use, you will need to obtain permission directly from the copyright holder. To view a copy of this licence, visit <http://creativecommons.org/licenses/by-nc-nd/4.0/>.

intraocular drug implants, etc.) or surgical methods (e.g. trabeculectomy, goniotomy, etc.) have been shown to be effective in preventing vision loss [4]. However, many patients continue to experience vision loss despite well-controlled IOP clinically, suggesting that there are other processes in the inner retina and optic nerve head that could drive vision loss [6–8]. Some of these include neuroinflammation (astroglial and microglial activation, complement factors, etc.), vasoactive peptides and signaling molecules (e.g. endothelin-1 and nitric oxide interplay), and cytokines (e.g. TNF α) [9–11]. There is a need for novel therapeutics that can directly protect RGCs and axons to preserve vision in the long-term for glaucoma patients, in addition to IOP lowering therapies.

While glaucoma patients are diagnosed in the clinic using the structural characteristics mentioned above (including RNFL thinning and ONH cupping) by OCT, their clinical records are often either incomplete, sparse with long intervals between readings, variable, and/or non-transferrable between practices. This issue is exacerbated when patients sign up for willed-organ donation and donate their eyes post-mortem to qualified eye banks for research purposes, as records accompanying donor tissues may not include detailed deidentified clinical information, especially in the United States. In addition, some post-mortem donor eyes (~ up to 20% in our experience) that are classified as non-glaucomatous according to medical records often show glaucoma-like characteristics after detailed histopathological examination, and thus may be mis-diagnosed. These confounders increase the challenge in accurately defining the glaucomatous disease stage of donated donor eye tissues after they have been processed for histopathology. Furthermore, pre-analytical variables such as fixatives used for histopathologic processing can introduce artifactual cupping of the optic disc. Appropriate staging and comparison to control samples is critical when evaluating changes in molecular pathways during the course of disease using techniques such as RNAScope or immunohistochemistry (IHC), as linking a particular pathway or potential therapeutic target to the stage of disease can be critical in determining when and where to therapeutically intervene. The use of post-mortem ocular tissue is critical in ophthalmic discovery research, as local assessment of potential drug targets at the site of disease pathogenesis is rarely possible in patients.

Recently, reports have described interesting observations regarding neuroinflammation in glaucomatous optic nerves/RGCs from human donor eyes and have compared and corroborated these findings to relevant preclinical models of glaucoma [12, 13]. These studies utilized histological assessments of ON atrophy, RGC numbers, and fibrosis in the ONH to define disease and

to compare the extent of neuroinflammation, neutrophil infiltration and microglia/macrophage changes (CD163⁺ or CD68⁺ immunoreactivity), across glaucomatous vs. non-glaucomatous donor eyes. In the current study, we used hallmarks of RGC loss and gliosis to develop a quantitative multi-parametric and systematic grading system for post-mortem human glaucoma eye tissue sections. Structural assessments and measurements were made both in the central retina (macula) and temporal retina as well as the ONH, using the Bruch's membrane opening (BMO) as the landmark. We then used linear regression and principal component analyses to study correlations between the RGC soma marker RBPMS [14], the RGC axonal marker neurofilament light chain (NEFL) [15, 16], the microglia/macrophage marker IBA1 [17], and the astrocyte marker glial fibrillary acidic protein (GFAP) [18, 19]. Our findings reveal that a quantitative structural and molecular marker grading approach can stratify post-mortem glaucoma samples into at least three severity groups, and this type of approach may be useful for researchers aiming to maximize insights derived from eye bank donor tissue.

Materials and methods

Human donor eye acquisition, processing, and IHC

Thirty-one human eye globes (HEGs) from consented donors with no history of glaucoma and twenty-one HEGs with an accompanying medical history of glaucoma but no detailed clinical information were collected from the Lion's Eye Institute for Transplant & Research (Tampa, FL) between 2017 and 2022. Donor demographics and recent medical history are listed in Table 1. The HEGs were enucleated within 6 h post-mortem and evaluated as not meeting the criteria for transplantation owing to low corneal endothelial cell count. All samples were shipped in Modified Davidson's Fixative (MDF: 9–10% formalin, 5% glacial acetic acid, 15% ethanol) and fixed for 48 h, and then transferred to 70% alcohol for 48–72 h. The tendinous attachment of the superior oblique muscle (indicating the superior and lateral aspect of the posterior globe), the fleshy muscular attachment of the inferior oblique muscle over the macula (indicating the lateral aspect of the globe) and the optic nerve stump (indicating the medial aspect of the posterior globe) provided 3 points of orientation (superior, medial, lateral) for the laterality of the globe. HEGs were cut transversely in the pupillary-optic axis into 3 parts with the optic nerve and macula contained in the central part and then embedded in paraffin in a Tissue-Tek[®] VIP[™] 5E-F2 processor (Sakura Finetek USA). 5-micron transverse sections with macula and the optic nerve were cut from the central part. These sections were then processed using standard dehydration, deparaffinization and rehydration

Table 1 Donor demographics

Donor #	Disease state	Age	Eye	Sex	Race/ethnicity	Recent medical history	Used for IHC portion of study
1	Non-glaucoma	81	OS	male	Caucasian	Acute cardiac crisis	No
2	Non-glaucoma	73	OS	male	Caucasian	Leukemia	Yes
3	Non-glaucoma	84	OS	male	Caucasian	Acute cardiac crisis	Yes
4	Non-glaucoma	92	OS	male	Caucasian	Cardiac arrest	Yes
5	Non-glaucoma	72	OS	male	Caucasian	Colon cancer	No
6	Non-glaucoma	84	OS	female	Caucasian	Multiple myeloma	Yes
7	Non-glaucoma	77	OS	male	Caucasian	Sepsis	Yes
8	Non-glaucoma	94	OS	male	Caucasian	COPD	Yes
9	Non-glaucoma	84	OS	male	Caucasian	Severe PVD	Yes
10	Non-glaucoma	78	OS	male	Caucasian	CHF, CVA	Yes
11	Non-glaucoma	79	OS	female	Caucasian	Leukocytosis, bowel perforation	No
12	Non-glaucoma	90	OS	female	Caucasian	Hospice care, failure to thrive	No
13	Non-glaucoma	74	OS	male	Caucasian	Colon cancer, cirrhosis	No
14	Non-glaucoma	76	OS	male	Caucasian	COPD	No
15	Non-glaucoma	83	OS	female	Caucasian	Trauma, hospice	Yes
16	Non-glaucoma	84	OS	male	Caucasian	End stage lung cancer	No
17	Non-glaucoma	88	OS	female	Caucasian	Pneumonia	Yes
18	Non-glaucoma	83	OS	female	Caucasian	Lung cancer with mets, pneumonia	Yes
19	Non-glaucoma	83	OS	female	Caucasian	Lung cancer, atrial fibrillation	Yes
20	Non-glaucoma	68	OS	male	Hispanic	Cellulitis of leg, severe PVD, limb ischemia	Yes
21	Non-glaucoma	80	OS	male	Caucasian	Acute cardiac crisis	No
22	Non-glaucoma	92	OS	female	Caucasian	Pneumonia, respiratory failure	No
23	Non-glaucoma	97	OS	female	Caucasian	Fecal impaction, weakness, pleural effusion	No
24	Non-glaucoma	99	OS	female	Caucasian	Renal failure	No
25	Non-glaucoma	94	OD	female	Caucasian	Sepsis	Yes
26	Non-glaucoma	75	OS	male	Caucasian	Pancreatitis	Yes
27	Non-glaucoma	78	OS	male	Caucasian	Renal failure	No
28	Non-glaucoma	75	OS	male	Caucasian	Type 2 diabetes	No
29	Non-glaucoma	79	OS	female	Caucasian	Anemia, HTN, COPD	Yes
30	Non-glaucoma	97	OS	female	Caucasian	Acute cardiac event	No
31	Non-glaucoma	77	OS	female	Caucasian	Cardiac event	No
32	Glaucoma	73	OS	male	Caucasian	Prostate cancer	Yes
33	Glaucoma	86	OS	male	Caucasian	Metabolic encephalopathy	Yes
34	Glaucoma	87	OS	male	Caucasian	Skin cancer	Yes
35	Glaucoma	97	OS	male	Caucasian	Acute cardiac crisis	Yes
36	Glaucoma	76	OS	female	Caucasian	MRSA	Yes
37	Glaucoma	65	OS	female	Caucasian	COPD, pneumonia	Yes
38	Glaucoma	79	OS	female	Caucasian	Pneumonia	Yes
39	Glaucoma	92	OD	female	Caucasian	Acute myeloid leukemia	Yes
40	Glaucoma	78	OS	female	Caucasian	Pneumonia	Yes
41	Glaucoma	77	OS	male	Caucasian	COPD, pneumonia	Yes
42	Glaucoma	93	OS	male	Caucasian	Pancreatic cancer	Yes
43	Glaucoma	88	OS	male	Caucasian	Renal failure	Yes
44	Glaucoma	80	OS	female	Caucasian	Acute myeloid leukemia	Yes
45	Glaucoma	68	OS	female	Black	Ichthyophthirius multifiliis	Yes
46	Glaucoma	83	OS	male	Asian	Fecal impaction, Weakness, Pleural effusion	Yes
47	Glaucoma	90	OS	male	Caucasian	Acute cardiac event	Yes
48	Glaucoma	85	OS	female	Caucasian	Acute kidney injury	Yes

Table 1 (continued)

Donor #	Disease state	Age	Eye	Sex	Race/ethnicity	Recent medical history	Used for IHC portion of study
49	Glaucoma	77	OS	female	Caucasian	COPD, respiratory failure	Yes
50	Glaucoma	71	OS	male	Caucasian	COPD, pneumonia	Yes
51	Glaucoma	70	OD	male	Caucasian	COPD, dementia	Yes
52	Glaucoma	78	OD	female	Caucasian	Intracerebral bleed	Yes

procedures and stained with hematoxylin and eosin (H&E). Sections were also assigned an AMD grade using criteria previously described [20]. IHC was performed with antibodies (Table 2) against RBPMS (RGC soma marker), NEFL (RGC axon marker), GFAP (astrocyte marker) and IBA1 (microglia/macrophage marker) using a LeicaBond RX stainer (Leica Biosystems, Deer Park, IL, USA). Heat induced epitope retrieval was performed in a solution of EDTA based epitope retrieval solution (HIER, pH 9.0) (AR9640, LeicaBond) at 95 °C for 20 min.

Image analysis and quantification

IHC stained slides were scanned at 20X magnification using an Aperio AT2 scanner (Leica Biosystems) and subsequently imaged and quantified using the HALO image analysis platform (Indica Labs, New Mexico USA). For colorimetric stains, regions of interest (ROIs) were defined over positively stained areas (purple or teal), and thresholds set based on these ROIs. The same thresholding settings were applied to all assessed images, and were set such that the stains of interest could be distinguished from light blue-stained nuclei (hematoxylin staining). Bruch's membrane opening (BMO) was used as a landmark for the optic nerve. IHC signals in the ganglion cell complex (GCC, including nerve fiber layer, ganglion cell layer, and inner plexiform layer) were collected from the central region (1 mm range from temporal BMO), peripheral retina (2 mm area beginning 7 mm from temporal BMO) and ONH (1 mm area below the line of the two sides of the BMO). RGC cells were counted from 5 mm range of the periphery (5 mm area beginning at 7 mm from temporal BMO) and 1 mm in the central

retina (1 mm from the temporal BMO) (Supplemental Fig. 1).

Statistical analysis and glaucoma disease stratification

Descriptive statistics and hypothesis testing

Tissue regions positively stained for NEFL, GFAP, and IBA1 were expressed as a percentage of positively stained area per total area measured. Retinal ganglion cells are reported as number of RBPMS positive cells per 6 mm of length of the retina. GCC thickness was measured in the central temporal region and reported as μm . Differences in NEFL, GFAP, IBA1, RBPMS and retinal thickness are reported as scatter plots with individual values from each donor, with horizontal lines indicating the mean \pm standard deviation. The distribution of data was assessed using the Kolmogorov–Smirnov test, and the normality of distribution was confirmed. Comparison between glaucomatous and non-glaucomatous groups were performed by unpaired t-test with $p < 0.05$ as statistically significant (* $p < 0.05$, ** $p < 0.01$, *** $p < 0.001$, **** $p < 0.0001$). Subsequently, due to the binary nature of the groups and in order to determine if the differences between the two groups were true, we performed the receiver operating characteristic (ROC) curve analysis. The degree of separability between sensitivity (true positive) and specificity (false positive) are indicated by the area under the curve (AUC) on the graphs. Next a linear regression analysis was performed to study the correlation between RBPMS:IBA1, RBPMS:NEFL, RBPMS:GFAP, and IBA1:GFAP comparing glaucomatous and non-glaucomatous donors. Goodness of fit and correlation is expressed by the R^2 value.

Table 2 Antibody information

Antibody	Vendor	Catalog #	Host and type	Stock concentration ($\mu\text{g/ml}$)	Dilution factor
RBPMS	Novus	NBP2-20112	Rabbit polyclonal	1000	1:800
NEFL	Proteintech	12998-1-AP	Rabbit polyclonal	600	1:1000
GFAP	Abcam	Ab7260	Rabbit polyclonal	1000	1:6000
IBA1	Wako	019-19741	Rabbit polyclonal	1000	1:5000

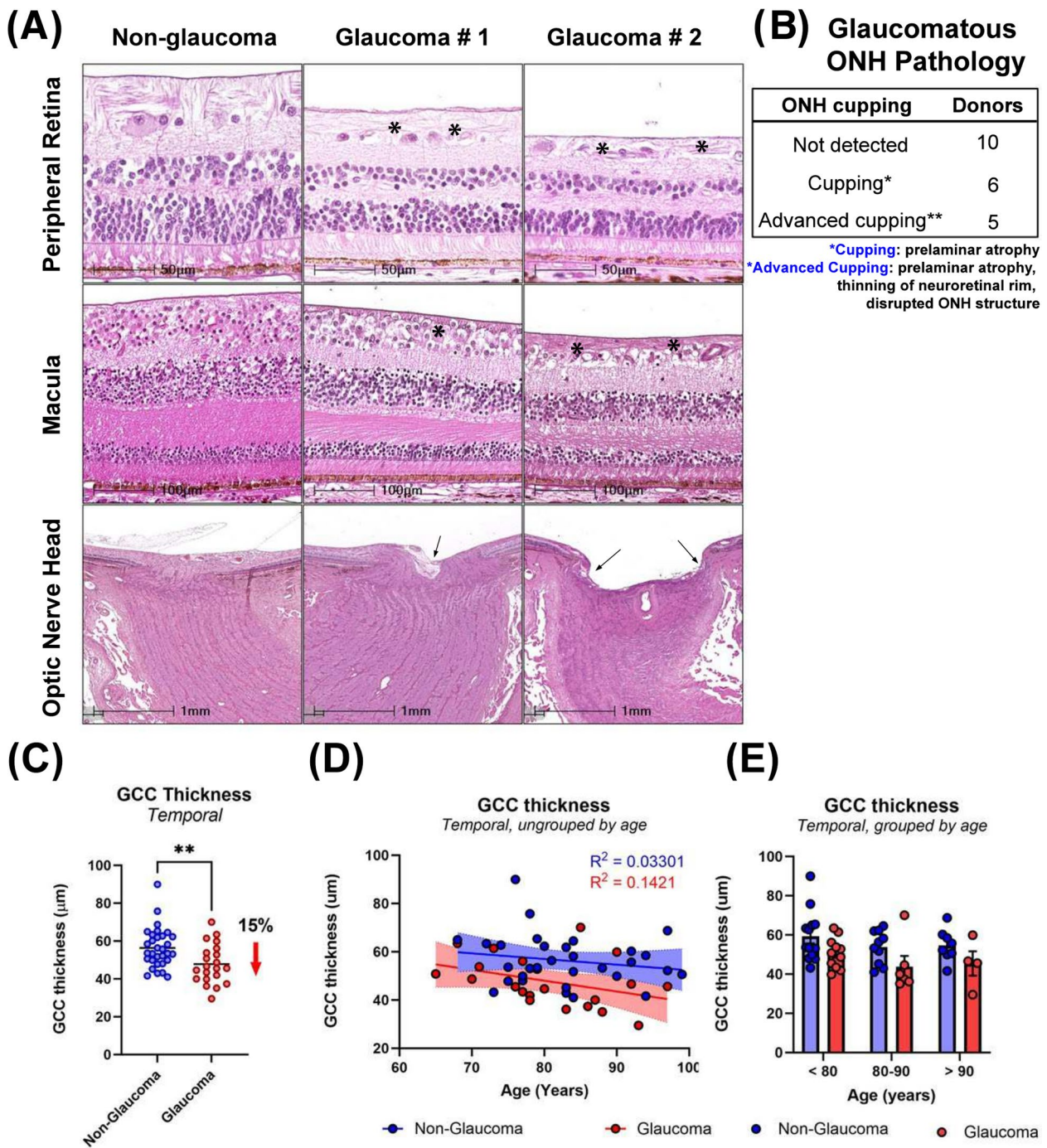


Fig. 1 Pathological changes of human glaucomatous retina and ONH. **A** Histological changes demonstrating decrease in peripheral retinal thickness, macular RGC loss, reduced RGC cell density, GCC thickness, ONH cupping in glaucoma. Asterisks in top and middle panels indicate thinning of the RNFL and arrows in the bottom panels demonstrate cupping. **B** ONH cupping or advanced cupping was often seen in glaucoma, which showed prelaminar atrophy, disrupted structures in optic nerve head and in optic nerve, and lamina cribrosa bowed posteriorly. **C** Scatter dot plot represents the individual temporal GCC thickness values for non-glaucomatous (n=31) and glaucomatous (n=21) donor tissues. GCC thickness was significantly decreased by 15% in temporal peripheral retina of glaucomatous donors. Horizontal bars indicate mean ± standard error of the mean. **p < 0.01, unpaired t-test. **D** GCC thickness does not decrease with age in non-glaucomatous or glaucomatous donors ($R^2 = 0.1421$, $R^2 = 0.03301$) **E** No statistically significant differences in GCC thickness observed comparing glaucoma and non-glaucoma donors when samples were binned by age. Data are mean ± SEM

Disease stratification

In order to further understand the data, we sought to determine if performing multivariate analysis and data clustering could classify the data by disease severity. First, we performed principal component analysis (PCA) from a data matrix consisting of 38 samples (16 non-glaucoma, 21 glaucoma donors) and 4 variables (NEFL, RBPMS, GFAP, IBA1). The data matrix was centered and normalized to get a mean value of zero and a standard deviation of 1 for each variable. A correlation matrix was calculated, and the eigenvectors and corresponding eigenvalues were extracted. The relative percentage of variance of each eigenvalue was quantified and diagrammed in a Scree plot (Fig. 8A) [21]. The selection of the number of principal components used was performed using the Kaise-Guttman criteria [22], using the eigenvectors whose corresponding eigenvalues had a value greater than 1. Subsequently, the score matrix was calculated by multiplying these eigenvectors by the square root of the corresponding eigenvalue. Following PCA, the score matrix was rotated orthogonally using Varimax [23] to extract the latent factors. The factor loading matrix was obtained from the rotated factor score matrix by matrix operations. The factors were interpreted by associating the variables with highest weights in each factor and expressed as a score plot (Fig. 8B). PCA combined with factor analysis revealed that 3 predominant variables contributed to maximal variance in the samples (i.e. NEFL, RBPMS, and GFAP). Finally, by applying the Calinski-Harabasz criterion [24] for unbiased k-means clustering, we determined the optimal number of clusters for both non-glaucomatous and glaucomatous donors, using the 3 variables identified, and the data was clustered and represented as 3D plot.

Results

In order to determine the extent of glaucomatous damage in the posterior segment of donor eyes, we systematically evaluated histological features from 21 glaucomatous eyes (65–97 years old) and 31 age-matched non-glaucomatous control eyes. The histologic parameters evaluated were the thickness of the GCC, cupping of the optic disc, number of remaining RGC soma, immunoreactivity of NEFL in retinal and optic nerve sections, and glial activation (immunoreactivity for GFAP and IBA1). At this stage, since limited clinical and medical histories of the donors were available to us, the donors remained unstratified.

Gross anatomical changes in retina, macula, and optic nerve head in glaucoma

Macular damage in samples with a positive medical history of glaucoma was observed by a discernible reduction in RGC cell numbers and density within the temporal macular region from H&E in 11 of 21 donors (Fig. 1A). In some donors, the RGC layer was completely lost in both temporal and nasal macular regions (Supplemental Fig. 2A) accompanied by local RGC loss in the central macula for one donor (Supplemental Fig. 2B). Cupping of the optic disc was observed in 11 of 21 glaucomatous donor eyes (Fig. 1B). Remodeling of the lamina cribrosa (compression and disorganization of the prelaminar, lamina and post-lamina regions) was observed in 13 of 21 donor eyes. The extent of cupping and lamina cribrosa remodeling varied between donors and did not always correlate with RGC loss [25–28]. Given that sample fixation and processing for histology could confound accurate assessment of cupping, we did not consider cupping for additional sample classification or stratification. We did not observe consistent changes in other layers of the macula, including the retinal pigment epithelium, suggesting that the observed changes relate to glaucoma, and not other conditions such as age-related macular degeneration.

Next, we compared GCC thickness of non-glaucomatous and glaucomatous retinas from donors (Fig. 1C-E). Qualitative thinning of the peripheral retina (RGC loss, RNFL thinning) was observed by H&E staining (Fig. 1A) in 12 of 21 glaucomatous retinas. We next directly evaluated RGC soma loss in the peripheral retina comparing temporal to macular regions, and the nasal to central area (between macula and ONH). RGC loss was noted in both regions around the macula (the temporal and nasal) from 8 of 12 donors with retinal thinning, but only in the temporal retina of the remaining 4 donors with thinning. To confirm reduction of RNFL thickness in glaucoma, GCC thickness was measured in the temporal peripheral retina of all donor retinas (temporal to macula, 7 mm from BMO, Supplemental Fig. 1). On average, the GCC thickness of non-glaucomatous eyes was $56.3 \pm 1.9 \mu\text{m}$ (mean \pm SEM) while it was significantly lower by 15% ($47.8 \pm 2.30 \mu\text{m}$) in glaucomatous eyes (Fig. 1C). Across donors, we observed no significant association of GCC thickness with age ($R^2=0.03301$ for non-glaucoma, $R^2=0.1421$ for glaucoma, Fig. 1D). When samples were stratified into 3 age groups (<80y, 80-90y, >90y) we did not observe any statistically significant differences in GCC thickness between glaucoma and non-glaucoma donors, when compared within or across groups (Fig. 1E). Together, the data demonstrate that while there is a statistically significant difference in temporal GCC thickness between groups in this cohort, we did not observe

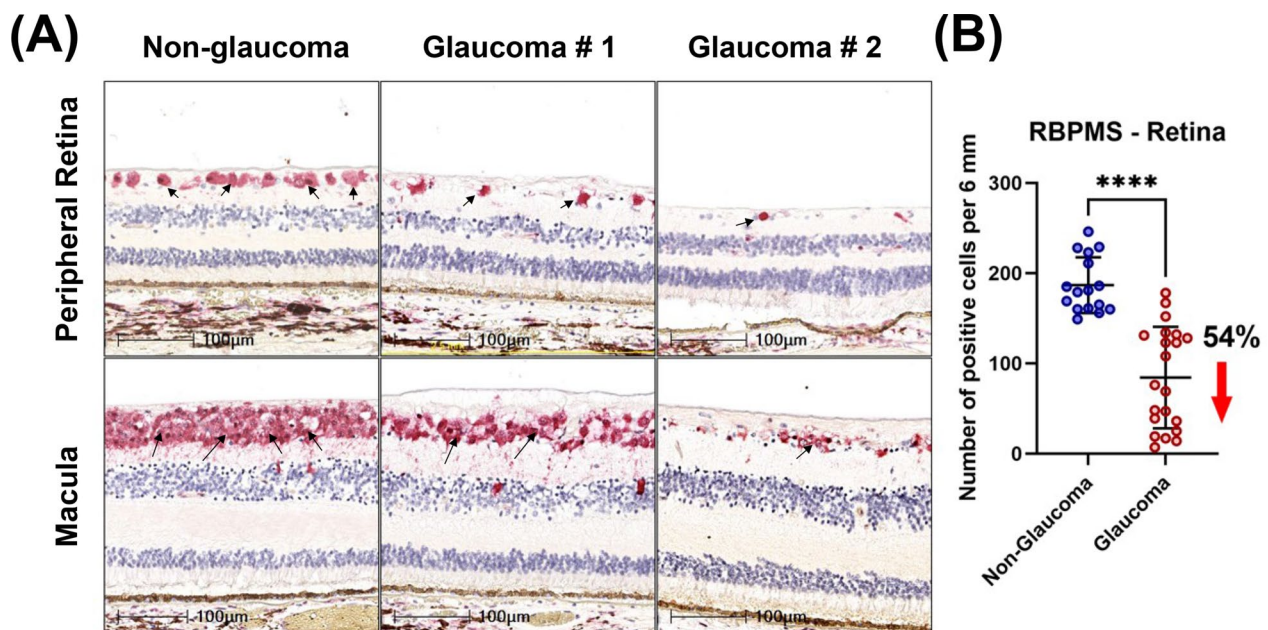


Fig. 2 RGC loss in glaucomatous donors observed by loss of RBPMS positive cells. **A** Loss of RGCs in peripheral retina and macula was observed in glaucomatous donors; arrows indicate RBPMS positive cells. **B** Scatter dot plot represents the individual values of RBPMS-positive RGCs (RBPMS + RGCs) for non-glaucomatous ($n=16$) and glaucomatous donor tissues ($n=21$). Quantitative analysis demonstrated a 54% reduction in RBPMS + RGCs in glaucomatous temporal peripheral retina. Horizontal bars indicate mean \pm standard deviation. **** $p < 0.0001$, unpaired t-test

clear age-associated trends, suggesting that disease is the primary driver of the observed differential.

Loss of retinal ganglion cells in glaucoma

To confirm RGC loss observed by H&E staining, we immunolabelled a randomized subset of non-glaucomatous and all glaucoma donor tissues with the RGC specific marker, RBPMS. Similar to our prior assessments, we observed 5–7 layers of RBPMS + RGCs in non-glaucomatous donors. However, in glaucomatous donors, most sections exhibited 2–5 RBPMS + cell layers. In some cases, there were only 0–2 layers suggesting advanced severity (Fig. 2A). Further quantitative analysis was performed in the temporal peripheral retina (5 mm from the end of the macular outline, Supplemental Fig. 1). We observed a 54% decrease in RGC density in the temporal peripheral retina from glaucomatous donors compared with non-glaucomatous donors (Fig. 2B).

Axonal and dendritic loss in glaucoma

Loss of axonal integrity and dendrites in the neural retina was determined by measuring the immunoreactivity of neurofilament light chain protein (NEFL) in both the peripheral temporal retina and ONH. Qualitative evaluation revealed a reduction in NEFL + processes in the peripheral temporal neural retina accompanied by irregular distribution of NEFL in the glaucomatous ONH (Fig. 3A). Expression levels of NEFL were quantified

within a 2 mm peripheral temporal region and 1 mm central region between the BMO and macula by normalizing the percentage positive immunolabel to total area measured. Normalized NEFL immunoreactivity in non-glaucomatous donor retina was $62.6 \pm 11.5\%$, while it was significantly reduced to $37.1 \pm 20\%$ in glaucoma (Fig. 3B) demonstrating a net reduction of NEFL + axons by 40%. The reduction in NEFL immunoreactivity in glaucomatous ONH was similar (42.4%) (Fig. 3B).

Glial activation in glaucoma

Qualitative assessment revealed increased immunoreactivity of GFAP in the glaucomatous peripheral retina accompanied by disorganized GFAP + regions within the ONH, compared with non-glaucomatous donors. Specifically, in non-glaucomatous tissues, when GFAP + signals were observed, these were localized to inner layers of the retina (especially in RNFL and RGCL) and around blood vessels. However, in glaucomatous tissues, the intensity of GFAP labelling was significantly higher and extended from the inner retina to the inner nuclear layer (INL), outer plexiform layer (OPL), and in some cases, to the outer nuclear layer (ONL) (Fig. 4A). Also, increased GFAP intensity was observed in glaucomatous ONH throughout the peripapillary, prelaminar and lamina cribrosa regions. Disorganized GFAP staining patterns were also observed in post-laminar regions of glaucomatous

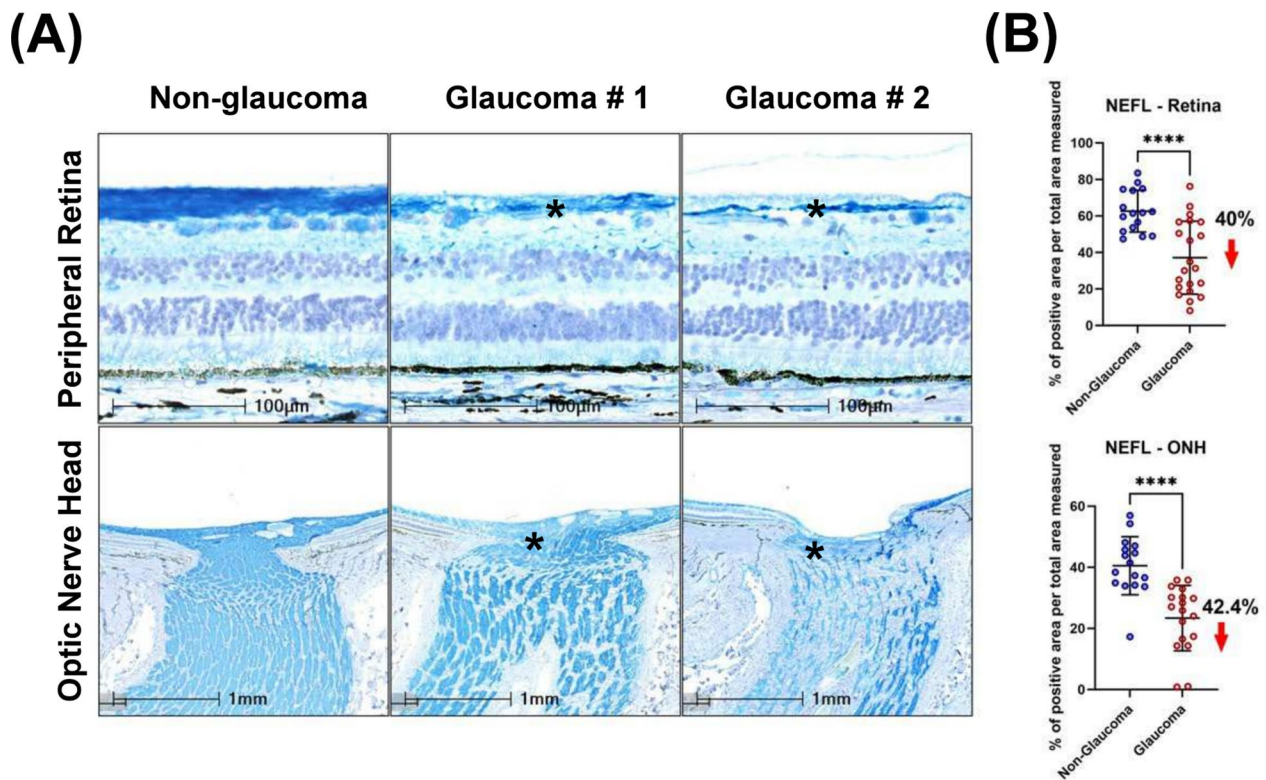


Fig. 3 Axonal and dendritic loss of RGCs visualized by NEFL immunolabelling in the peripheral retina and ONH. **A** Decreased NEFL expression in temporal peripheral retina and ONH, and disorganization of NEFL immune staining was observed in glaucomatous tissues. Asterisks indicate representative areas with loss of NEFL. **B** Scatter dot plot represents the individual values of neurofilament light chain (NEFL) for non-glaucomatous (retina, $n = 16$, ONH, $n = 16$) and glaucomatous donor tissues (retina, $n = 21$; ONH, $n = 18$). Quantitation of NEFL staining showed a statistically significant reduction in the temporal peripheral retina (40%) and optic nerve head (42.4%) of glaucoma donors. Horizontal bars indicate mean \pm standard deviation. **** $p < 0.0001$, unpaired t-test

ONH (Fig. 4A). Using a similar quantitative approach to NEFL measurement, we report a 64% increase in normalized GFAP-immunoreactivity in glaucomatous temporal peripheral retina compared with non-glaucomatous donor retinas (Fig. 4B). Similar increases in GFAP immunoreactivity were seen in the ONH (80.6%).

Next, we evaluated the number of microglia present in the tissue by immunolabelling for IBA1+ cells. In glaucomatous retinas, IBA1+ microglia were mostly present in the RNFL, ganglion layer, IPL and INL (Fig. 5A). Dual staining of IBA1 and RBPMS detected IBA1+ cells to be closely associated with RBPMS+RGCs (Supplemental Fig. 3). A significantly greater cell density (% positive cells per total area measured) of IBA1+ microglia was observed in glaucomatous retinas ($7.8 \pm 3.7\%$) compared with non-glaucomatous tissues ($4.1 \pm 1.3\%$; Fig. 5B) reflecting a net increase of 90.9%. In the optic nerve head (within the first 1 mm below BMO, a significant increase in IBA1 positive cell density was observed in glaucomatous tissues compared with non-glaucomatous tissues (58.4%; Fig. 5B).

Stratification of disease severity by multivariate analysis

After assessing individual markers, we sought to determine if there was any correlation between them. First, we asked if there was any correlation between protein marker staining between the retina and optic nerve head tissues. This analysis was performed only on sections from donors where both the retina and optic nerve were present. Spearman's analysis demonstrated a statistically significant correlation for GFAP and NEFL immunolabelling between the retina and optic nerve head, but no statistical significance was observed for IBA1 labelling between the two tissues (Fig. 6). For all subsequent analyses, measurements from only the retinal tissue were used.

Since loss of RGCs is considered a hallmark of disease, we performed all our Spearman correlation analyses against quantitative RBPMS+immunoreactivity in the temporal retina. We observed a positive correlation between loss of NEFL+immunoreactivity and loss of RBPMS+RGC cell density ($R^2 = 0.8153$; Spearman correlation, Fig. 7A) in glaucomatous tissues. This was a significant increase when comparing the same

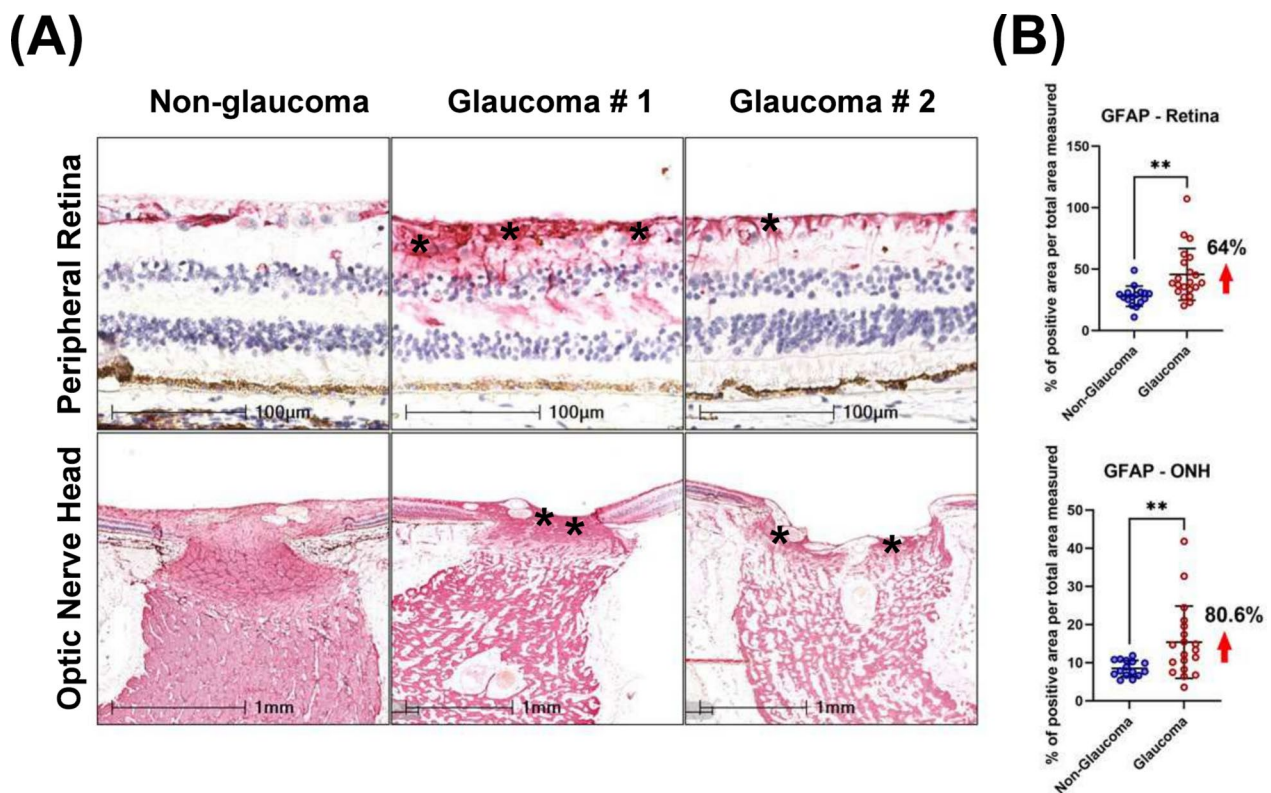


Fig. 4 Detection of activated astrocytes by GFAP immunoreactivity. **A** Compared with non-glaucomatous donors, upregulation of GFAP was detected in glaucomatous peripheral retina and ONH. Arrows indicate representative GFAP immunoreactivity. Asterisks on the bottom panel highlight the region of the ONH quantified in Fig. 4B. **B** Scatter dot plot represents the individual values of reactive astrocytes (GFAP + cells) for non-glaucomatous (retina, $n = 16$; ONH, $n = 16$) and glaucomatous donor tissues (retina, $n = 21$; ONH, $n = 19$) assessed by histology. Quantitative analysis showed that GFAP was significantly upregulated in the temporal peripheral retina (64%) and optic nerve head (80.6%) of glaucoma donors. Horizontal bars indicate mean \pm standard deviation. ** $p < 0.01$, unpaired t-test

parameters in non-glaucomatous donors ($R^2 = 0.3648$; Spearman correlation). No significant correlation was observed comparing RBPMS and GFAP or IBA1 levels in either glaucoma or non-glaucomatous donors. In the subset of donors where IBA1 positive immunoreactivity was observed, no relationship between GFAP and IBA1 immunostaining was observed in either glaucomatous or non-glaucomatous donors (Fig. 7B); although the variability in staining for both parameters was significantly greater for glaucomatous donors than non-glaucomatous donors.

Next, to determine the extent that donor variability contributed to the significance in quantitative measurements, and to compare sensitivity vs. specificity of the outcomes comparing glaucomatous and non-glaucomatous donors, we performed receiver operating characteristic (ROC) curve analysis (Supplemental Fig. 4). ROC analysis revealed that the area under the curve was the greatest for RBPMS (AUC = 0.9583) and those for NEFL (AUC = 0.8333), GFAP (AUC = 0.8274), and IBA1 (AUC = 0.8472) were significant, reinforcing the results

that the quantitative changes observed in glaucoma were true positives.

Since variability was observed both from the scatter and ROC plots, we hypothesized that these changes in temporal retinal NEFL (axonal & dendritic loss), RBPMS (RGC loss), and GFAP (glial activation) levels may be reflective of disease stage. PCA and factor analysis of the data revealed that the first two principal components with 3 variables (NEFL, RBPMS, and GFAP) contributed to the maximal variance (>85%) in the data (Fig. 8A, B). Using the quantitative measurements for these 3 variables, unbiased k-means clustering revealed 3 clusters for glaucoma samples and 2 clusters for non-glaucoma donors (Fig. 8C).

The two non-glaucoma clusters were predominantly factored on possessing a high level of RBPMS+ and NEFL+ staining, and a low proportion of GFAP+ glial cells. For glaucomatous tissues, the clustering was parameter dependent. Donor sections with the highest level of RBPMS+NEFL+ staining and least glial proliferation/GFAP positivity were categorized as mild glaucoma.

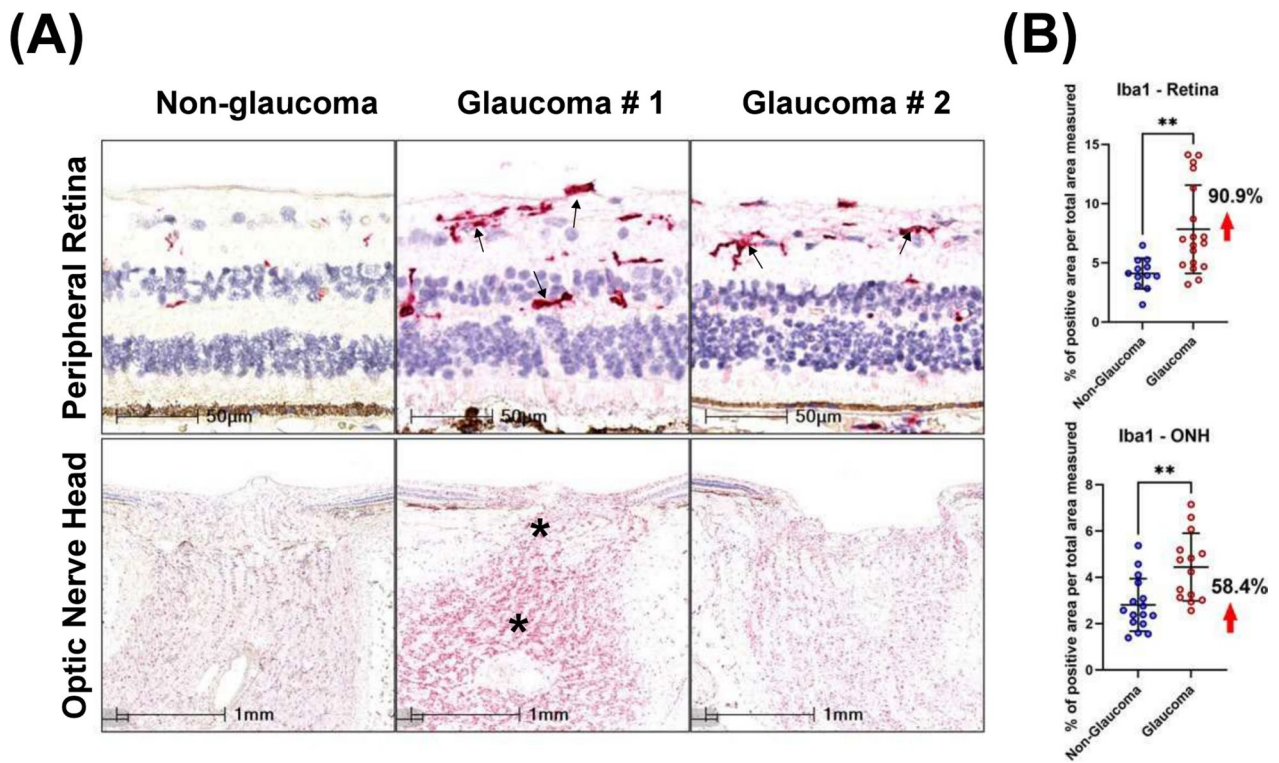


Fig. 5 Detection of microglia by IBA1 immunoreactivity. **A** IBA1 was upregulated in glaucomatous peripheral retina and ONH compared with non-glaucomatous donors. Arrows indicate IBA1 positive cells in the retina and asterisks increased IBA1 immunoreactivity in the ONH. **B** Scatter dot plot represents the individual values of IBA1 + cells for non-glaucomatous (retina, n = 12; ONH, n = 16) and glaucomatous donor tissues (retina, n = 18, ONH, n = 14) assessed by histology. Quantitative analysis of IBA1 positivity showed that IBA1 was statistically upregulated in the temporal peripheral retina (90.9%) and optic nerve head of (58.4%) glaucoma samples. Horizontal bars indicate mean ± standard deviation. **p < 0.01, unpaired t-test

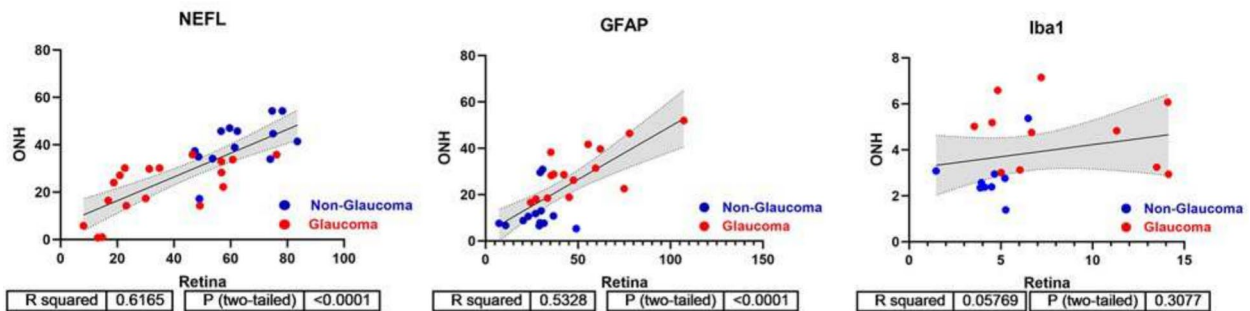


Fig. 6 Correlation analysis between retina and optic nerve head. Spearman's correlation and linear regression was performed for NEFL, GFAP and IBA1 expression comparing retina and ONH measurements for glaucoma and non-glaucoma donors. NEFL and GFAP exhibit strong correlation between retina and ONH measures ($R^2=0.6165$ and $R^2=0.5328$, respectively), but this is not the case for IBA1 ($R^2=0.3077$)

Donor samples with the greatest increase in GFAP + cells but moderate loss of NEFL + RBPMS + staining were classified as moderate glaucoma. Finally, donors with greatest loss of RBPMS + NEFL + staining but a persistence of

some GFAP + cells were classified as severe glaucoma. These data suggest a phasic stratification with disease where maximal glial activation is seen in the moderate stage.

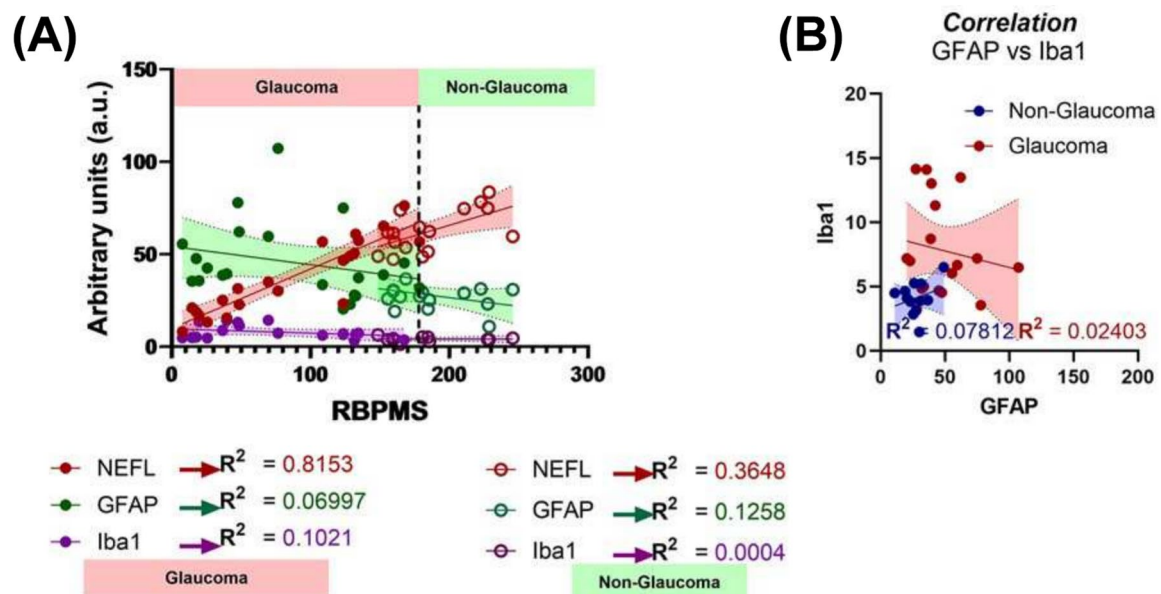


Fig. 7 Spearman's correlation analysis. **A** Spearman's correlation demonstrated maximal correlation between RBPMS and NEFL in glaucomatous donors, with minimal correlation seen when comparing other markers in glaucomatous and non-glaucomatous donor tissues. **B** No statistically significant correlation was observed when comparing GFAP and IBA1 immunoreactivity in the retina for both non-glaucomatous and glaucomatous donors

Changes in immunohistochemical markers stratified by glaucoma severity

After implementation of clustering and definition of the three distinct glaucoma groups, we reassessed our data based on this refined system. We observed a progressive loss in RBPMS+RGCs and NEFL staining in the temporal retinas with increasing glaucoma severity (Fig. 9A, B). GFAP+ cell density was severity-dependent, demonstrating maximal glial activation with moderate severity (Fig. 9C). On the other hand, IBA1+ immunoreactivity increased in the moderate and severe glaucoma groups with large variability but did not drastically decrease in severe glaucoma (Fig. 9D).

Discussion

Researchers often use post-mortem eyes obtained from eye banks to identify biomarkers and new therapeutic targets. A notable challenge in this approach is that longitudinal clinical imaging and detailed medical histories are typically not provided to eye banks in the United States, and experimental analysis relies heavily on self-disclosure of ocular disease history by the donor's family. Thus, there is a need to better stratify donor samples with incomplete histories to better understand the utility of the tissues for mechanistic investigation. In this study, we used multiparametric histological assessments, focusing on molecular markers, to classify glaucoma severity in post-mortem donor tissues.

There is currently no consensus for histology-based morphometric, RNA, and protein markers that accurately predict glaucoma stage. In addition, death-to-preservation time and fixation procedures can create confounding artifacts. Further, our simple morphometric analysis of GCC thickness showed a modest decrease in glaucoma samples, but was unable to provide additional information about potential disease stage. Thus, relying only on measurements of physical features could lead to a less accurate assessment of disease stage. We selected a combination of immunohistological measurements in the neural retina and ONH that we reasoned would give key estimates of severity: (1) the number of RBPMS+RGCs, to assess remaining RGC soma; (2) neurofilament staining as measured by NEFL, to assess the extent of axonal and dendritic loss; (3) the number of IBA1+ cells, to assess microglia/macrophages and estimate the degree of innate inflammation in the tissue, and; (4) the number of GFAP+ cells, to assess astrocytes and estimate the degree of gliosis in the tissue. Individual assessment of each marker showed a decrease of RBPMS and NEFL staining and an increase in IBA1 and GFAP staining in glaucoma samples, as expected. A factor to consider when grading is the consistency in available tissue area. While retinal regions could be consistently normalized, we observed significant variability in cupping and the amount of optic nerve and ONH tissue between

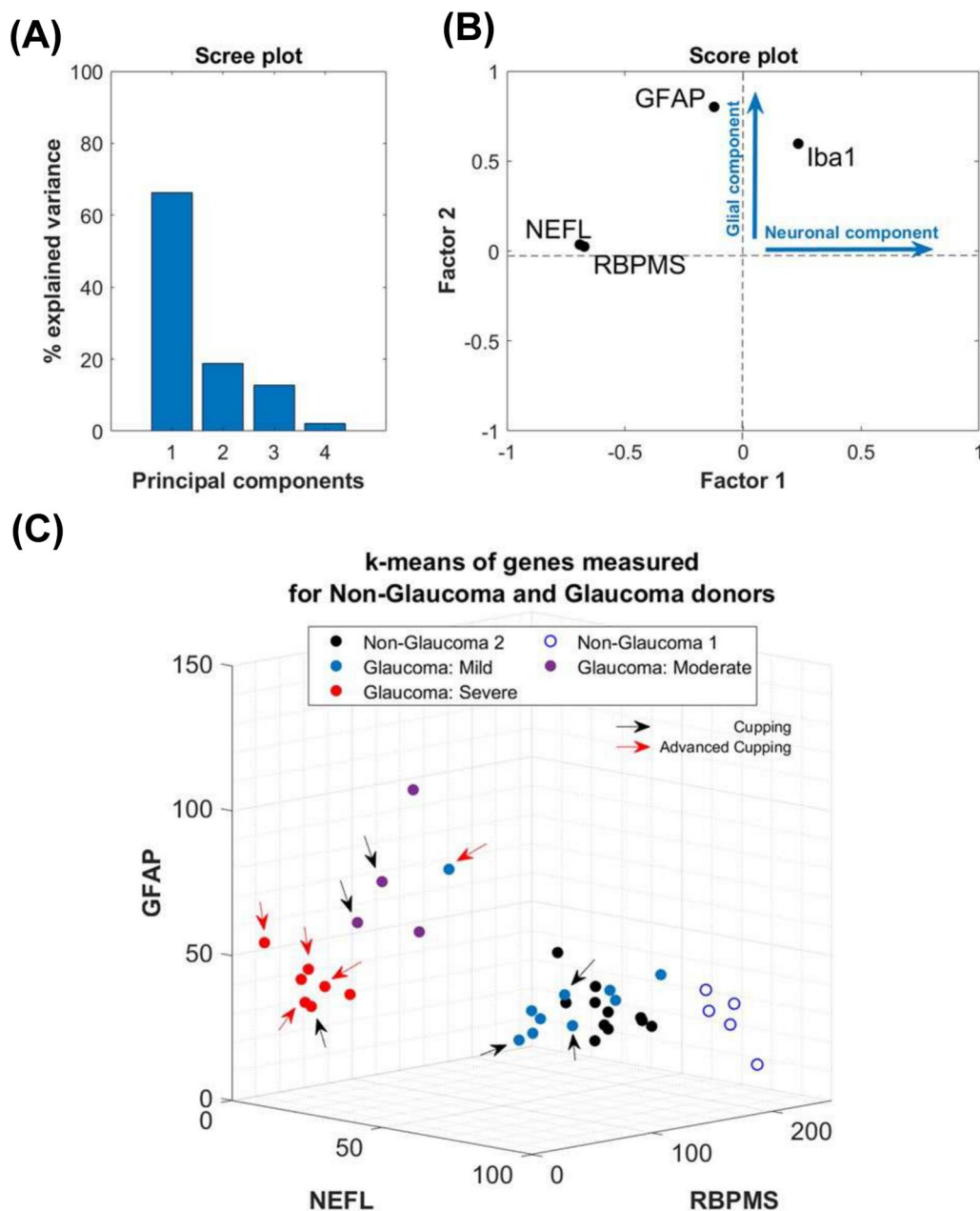


Fig. 8 Multivariate statistical analysis. **A** Principal component analysis for GFAP, RBPMS, NEFL and IBA1 immunoreactivity demonstrated that >85% of the variance in the data was contributed by the first 2 principal components, as indicated in the Scree plot. **B** Score plot from factor analysis showing that maximal variance was weighted by 3 factors: RBPMS, NEFL and IBA1, with the former 2 representing neuronal components, and the latter representing a glial component. **C** Cluster analysis using the principal components. Severity of glaucoma was assessed by applying the Calinski-Harabasz criterion for unbiased k-means clustering using the expression values for RBPMS, NEFL, and GFAP positive staining. Non-glaucomatous donors clustered in 2 distinct groups while glaucomatous tissues clustered in 3 distinct groups (mild, moderate, and severe). Arrows as indicated in the figure identify tissues with qualitative cupping of the ONH observed through histology

glaucomatous donor sections, which could impact normalization between donors. To minimize the effects of this potential confounder, we focused our quantitative assessments on retinal measurements. Combining all four quantitative measurements in a multiparametric

approach, we were able to stratify our glaucoma donor samples into three distinct groups of mild, moderate, and severe. This type of stratification was not attainable using donor records or individual markers. Our conceptual grading approach is outlined in Fig. 10.

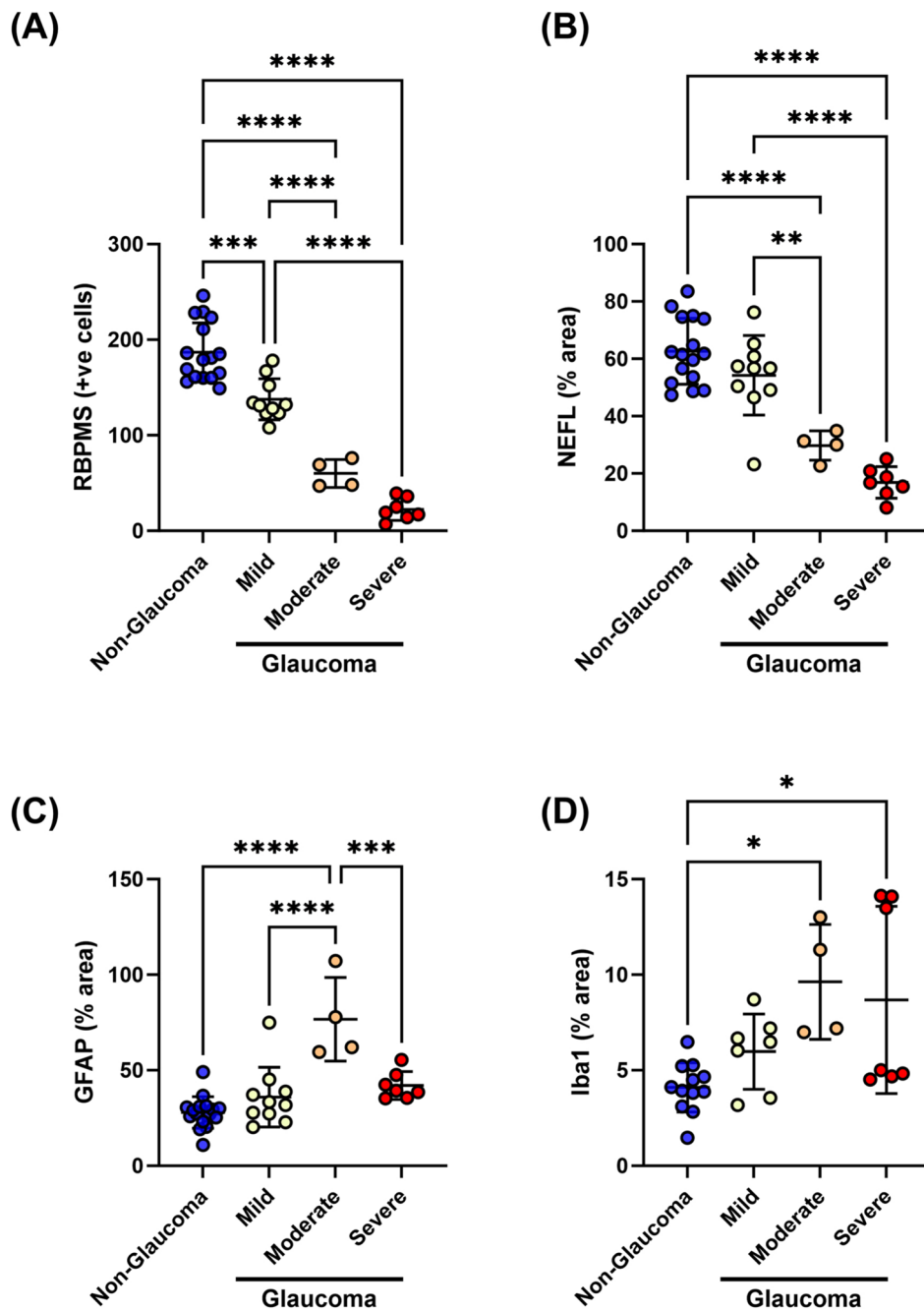


Fig. 9 Post-hoc analysis after stratification of glaucomatous donors. Progressive RGC degeneration and increased glial reactivity were observed in the retina with disease severity. **A** Loss of RBPMS + RGC cells, **B** loss of axons (NEFL), **C** increased astrocytic activation (GFAP), and **D** microglia/macrophage activation (IBA1) was stratified by disease state. Horizontal bars indicate mean \pm standard deviation. * $p < 0.05$, ** $p < 0.01$, *** $p < 0.001$, **** $p < 0.0001$, One-way Analysis of variance (ANOVA) followed by Tukey’s multiple comparison test

Glia (microglia, astrocytes and Müller glia) play roles either in restoring homeostasis or exacerbating disease conditions in neuropathies. Notable neuroinflammatory microglial changes include an increase in numbers, IBA1 + expression, and upregulation of complement factors such as C1Q and C3. Early microglial changes likely

involve synaptic pruning via complement deposition, followed by persistent pro-inflammatory phenotypes that indirectly promote neuroinflammation by engaging reactive astrocytes to secrete cytokines and vasoactive peptides such as endothelin-1 [9, 10, 29]. We observed a 90% increase in IBA1 + cells in glaucomatous donor retinas

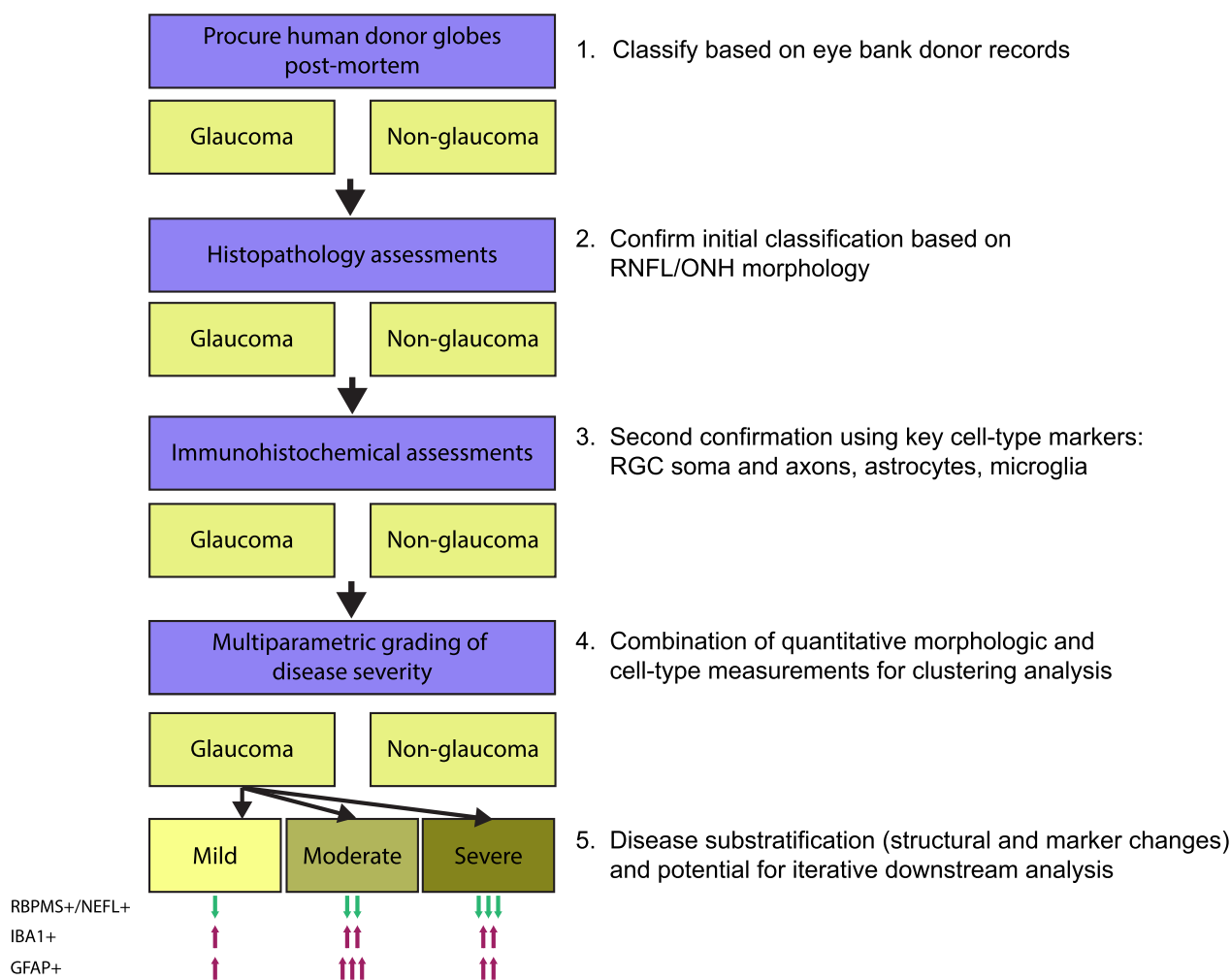


Fig. 10 Schematic of donor eye grading workflow. Conceptual outline of steps in acquisition and grading of post-mortem donor eyes, accompanied by qualitative descriptions of protein marker stain changes from non-glaucoma samples in each severity grade. Note that the evaluation of protein markers is confined to the temporal retina. One arrow indicates a mild/minimal change, two arrows indicate a moderate change, and three arrows indicate a severe/maximal change. The predominant/distinguishing features of each grade are: mild – pre-mortem history of glaucoma; moderate – maximal GFAP positivity in temporal neural retina; severe – maximal loss of RBPMS and NEFL positivity in temporal retina

compared to non-glaucomatous donors, with enrichment in the RGC and inner plexiform layers. The increase in IBA1+ cells was most pronounced in the moderate and severe glaucoma groups. In contrast, while the number of GFAP+ cells also increased in glaucoma, there was not a statistically significant correlation between GFAP+ and IBA1+ expression across glaucoma samples after stratification, suggesting a temporal disconnect between microglial and astrocyte activation, proliferation, and modulation over the course of disease progression. Alternatively, astrocyte activation could be different in the ONH, given that predominant glial activation changes in glaucoma have been observed in the unmyelinated region of the optic nerve. We did not evaluate molecular

changes in the ONH in this study, as its size varied between donors, and our initial classification of disease was based on the presence or absence of glaucoma from donor records. The implication of the temporal disconnect between activation of different glial cells is unclear, and further mechanistic studies may be required to delineate specific roles and spatial distribution in initiation and progression of neurodegeneration. We note that a recent literature meta-analysis [30] of molecular changes in human glaucomatous post-mortem retina and ON tissues confirmed associations of glial cell activation and neuroinflammation.

The explosion of highly multiplexed transcriptomics and proteomics platforms is enabling greater resolution

of molecular markers in human tissues. For example, a recent study [31] identified 37 clusters and subclusters of distinct cell types in the optic nerve, optic nerve head, retinal pigment epithelium and peripapillary sclera of non-glaucomatous donor globes. These findings offer insights into expression profiles that define cell subtypes. The potential to combine detailed molecular phenotypes with histopathological grading of glaucoma severity will likely be important in identifying disease and cell-type specific targets associated with distinct disease stages. For instance, the cell-type specific expression patterns of glaucoma risk genes (including primary open-angle and normotensive glaucoma) and genes that confer susceptibility to increased IOP but not glaucoma are distinct and different [30]. These studies were performed using non-glaucomatous donor tissues, and one could envision a similar assessment, accompanied by multiplexed spatial transcript and protein profiling, on samples graded with the severity index from our current study. This approach could identify novel targets and mechanisms of action and lead to new therapeutic hypotheses. For example, impairment in microglial autophagy has been noted in neurodegeneration and aging [32]. The differential expression profiles of microglial subtypes indicate of putative pro- and anti-neuroinflammatory roles, particularly when considering surface receptor profile changes. For instance, the CX3CR1 receptor appears to play a role in eliminating dead or dying cells like RGCs, and antagonism of this receptor exacerbates RGC loss via microglial activation in preclinical glaucoma models [33, 34]. Microglial adenosine A2A receptor or A3 receptor antagonism is neuroprotective in glaucomatous rodent *in vitro* and *in vivo* models [35, 36]. These examples suggest that profiling of cell surface receptor mRNA transcripts and protein levels may yield further insights when combined with multiparametric indexing of glaucomatous donor globes.

There are several gaps and limitations in our approach. First, we currently lack a sufficient number of samples to construct an independent validation cohort and have not yet performed a confirmatory exercise. Independent replication of our approach would test whether the results from donor samples obtained from one site are robust and reproducible. We do note that similar increases in immune/glia activation have been observed in other independent studies [12, 13]. Second, there is no current consensus on protein markers and the magnitude of change in these markers that can be used to reliably classify glaucoma disease severity. Third, our samples were fixed using MDF, as opposed to neutral buffered formalin (NBF), which is more widely used. MDF preserves the

attachment of the retina to the RPE, but it has been noted that some antigens are less well labelled in MDF when compared to NBF [37]. In our hands, the staining intensity of IBA1 and GFAP were comparable in MDF and NBF fixed eyes ($n=4$ per group, data not shown), but it remains possible that some antigens of interest, morphological features and fine cellular processes may vary in detectability between fixation conditions. Nonetheless, this suggests that researchers with NBF-fixed tissues would be able to use a similar grading approach. Fourth, the complexity of gliosis and neuroinflammation suggests that reliance on a few RNA or protein markers is unlikely sufficient to thoroughly describe the complexity of cell phenotypes in glaucoma. Identification of additional markers and subsequent incorporation into a grading scheme could further refine or potentially alter our classification scheme. Finally, the statistical approaches used to sub-stratify our samples could be further refined, or additional methods incorporated. We note that some of the statistical methods used may not be immediately accessible to some researchers and pathologists. Our grading framework provides a starting point for discussion and will enable further refinement, with the ultimate goal of building a consensus methodology for histology-based grading of glaucoma samples. As consensus is refined, development of automated classification systems could be pursued.

Looking ahead, there is still a disconnect between assessments that can be made in live patients and post-mortem ocular samples. It is challenging to obtain donor globes from eye banks with a rich set of longitudinal imaging and functional measurements, at least in the United States, and potentially in other localities. To correlate clinically observable changes across the course of glaucoma progression with terminal cellular and molecular measurements, bridging studies are needed. With recent developments in AI algorithms and available training datasets, it is more feasible that post-mortem histological assessments could be correlated with similar *in-life* measurements. For example, rapid grading of a larger number of clinical images of optic nerve heads can enable prediction of progression [38]. Paired studies of well-curated donor eyes accompanied by comprehensive longitudinal clinical information with less-well characterized donor eyes from eye banks, coupled with comprehensive multiplexed RNA and protein profiling, could serve as the basis for AI-based scoring. Such a resource could greatly enhance the research community's use of donor tissue and accelerate our ability to understand glaucoma progression at cellular and molecular resolution, in order to develop the next wave of neuroprotective therapies.

Supplementary Information

The online version contains supplementary material available at <https://doi.org/10.1186/s40478-024-01880-2>.

Supplementary material 1

Supplementary Figure 1: Schematic representation of regions utilized for quantitative histological analysis. Retinal thickness measured on H&E slides. Thickness of the Ganglion Cell Complex (GCC) including the retinal nerve fiber layer (RNFL) and retinal ganglion cell (RGC) layer plus inner plexiform layer was measured. 30–40 measurements were conducted in the 2 mm range of temporal peripheral retina (beginning from the single layer from the macula). Cell quantification: RBPMS+ cells in the 5 mm range of temporal retina were counted. Quantification of NEFL by area: The percentage area of the positive stained signal (%) of the total area measured in 2 mm range was calculated; vessels were excluded. Supplementary Figure 2: Variability observed between donors with a medical history indicating glaucoma. (A) The RGC layer was lost in both temporal and nasal macular regions in sections from this donor. (B) A second, different donor, exhibiting localized loss of RGCs and a reduction in RGC density in the central and temporal macula, respectively. Supplementary Figure 3: Representative images of co-staining of IBA1+ and RBPMS+ cells in glaucomatous donors. Peripheral retinas immunolabeled with RGC (RBPMS; red arrow) and microglial (IBA1; blue arrow) cell markers demonstrated that both cell types exhibited a close (proximity) association with each other (n=3). Supplementary Figure 4: Receiver operating characteristic curve analysis was performed to distinguish between false positive or false negative differences between values for glaucomatous and non-glaucomatous donors. ROC AUCs showed that expression levels of (A) RBPMS, (B) NEFL and (C) GFAP demonstrate significant differences between glaucomatous and non-glaucomatous donor tissues with RBPMS serving as the best indicator for disease discrimination.

Acknowledgements

We thank David Ammar, Nicholas Sprehe, Jason Woody and the team at Lion's Eye Institute for Transplant and Research (now Lion's World Vision Institute) for their partnership in donor tissue procurement, and Chenying Guo, Chia-Ling Huang, Nathaniel Kirkpatrick, Xiaoqiu Wu, and Junzheng Yang, for advice and support with sample grading and data analysis. Lastly, we would like to thank the donors and their families for their generous gift to research.

Author contributions

CX performed the majority of downstream tissue processing, sectioning, staining, image acquisition and histological measurements, and most histological analysis. VR performed all statistical analyses. YQ designed and implemented all tissue procurement, initial tissue processing, and sample and records management processes. MM performed some histological design, analysis and interpretation. JTD performed downstream tissue processing, sectioning, staining, image acquisition, and AMD stage assessments. CX, VR, MM, CLG, CWW and GP conceptualized, designed and interpreted the work. All authors wrote, read and approved the final manuscript.

Funding

Funding for this study was provided by Novartis Biomedical Research. The authors conducted the described work in the course of normal business as employees of Novartis.

Availability of data and materials

All data generated or analyzed during this study are included in this published article and its supplementary information files.

Declarations

Ethics approval and consent to participate

Deidentified post-mortem human eyes were procured by the Lions Eye Institute for Transplant & Research (LEITR; Tampa FL) with consent of donors or donors' next of kin and in accordance with the Eye Bank Association of America (EBAA) medical standards, applicable US/Florida law for human

tissue donation, the Declaration of Helsinki and FDA regulations, and Novartis guidelines regarding human tissue research.

Consent for publication

All human samples used in this manuscript were deidentified and are unattributable to specific individuals, so specific individual consent is not applicable.

Competing interests

CX, VR, YQ, MM, JTD, CLG, CWW and GP are all employees of Novartis and may hold stock.

Received: 29 May 2024 Accepted: 24 October 2024

Published online: 06 January 2025

References

1. Quigley HA, Broman AT (2006) The number of people with glaucoma worldwide in 2010 and 2020. *Br J Ophthalmol* 90:262–267
2. Tham Y-C, Li X, Wong TY, Quigley HA, Aung T, Cheng C-Y (2014) Global prevalence of glaucoma and projections of glaucoma burden through 2040: a systematic review and meta-analysis. *Ophthalmology* 121:2081–2090
3. Weinreb RN, Aung T, Medeiros FA (1901) The pathophysiology and treatment of glaucoma. *JAMA* 2014:311
4. Weinreb RN, Leung CKS, Crowston JG, Medeiros FA, Friedman DS, Wiggs JL, Martin KR (2016) Primary open-angle glaucoma. *Nat Rev Dis Primers* 2:16067
5. Yu M, Lin C, Weinreb RN, Lai G, Chiu V (2016) Leung CK-S: risk of visual field progression in glaucoma patients with progressive retinal nerve fiber layer thinning. *Ophthalmology* 123:1201–1210
6. Kass MA (2002) The ocular hypertension treatment study. *Arch Ophthalmol* 120:701
7. Group CN-TGS (1998) Comparison of glaucomatous progression between untreated patients with normal-tension glaucoma and patients with therapeutically reduced intraocular pressures. *Am J Ophthalmology* 126:487–497
8. Hejil A, Leske MC, Bengtsson B, Hyman L, Bengtsson B, Hussein M (2002) Reduction of intraocular pressure and glaucoma progression: results from the early manifest glaucoma trial. *Arch Ophthalmol* 120:1268–1279
9. Tezel G (2022) Molecular regulation of neuroinflammation in glaucoma: current knowledge and the ongoing search for new treatment targets. *Prog Retin Eye Res* 87:100998
10. Prasanna G, Krishnamoorthy R, Yorio T (2011) Endothelin, astrocytes and glaucoma. *Exp Eye Res* 93:170–177
11. Yorio T, Krishnamoorthy R, Prasanna G (2002) Endothelin: is it a contributor to glaucoma pathophysiology? *J Glaucoma* 11:259–270
12. Rutigliani C, Tribble JR, Hagström A, Lardner E, Jóhannesson G, Stålhammar G, Williams PA (2022) Widespread retina and optic nerve neuroinflammation in enucleated eyes from glaucoma patients. *Acta Neuropathol Commun* 10(1):118
13. Margeta MA, Lad EM, Proia AD (2018) CD163+ macrophages infiltrate axon bundles of postmortem optic nerves with glaucoma. *Graefes Arch Clin Exp Ophthalmol* 256:2449–2456
14. Rodriguez AR, de Sevilla Müller LP, Brecha NC (2014) The RNA binding protein RBPMS is a selective marker of ganglion cells in the mammalian retina. *J Comp Neurol* 522:1411–1443
15. Arslan B, Zetterberg H (2023) Neurofilament light chain as neuronal injury marker – what is needed to facilitate implementation in clinical laboratory practice? *Clin Chem Lab Med (CCLM)* 61:1140–1149
16. Gaetani L, Blennow K, Calabresi P, Di Filippo M, Parnetti L, Zetterberg H (2019) Neurofilament light chain as a biomarker in neurological disorders. *J Neurol Neurosurg Psychiatry* 90:870–881
17. Imai Y, Ibatata I, Ito D, Ohsawa K, Kohsaka S (1996) A novel gene *iba1* in the major histocompatibility complex class III region encoding an EF hand protein expressed in a monocytic lineage. *Biochem Biophys Res Commun* 224:855–862

18. Hol EM, Pekny M (2015) Glial fibrillary acidic protein (GFAP) and the astrocyte intermediate filament system in diseases of the central nervous system. *Curr Opin Cell Biol* 32:121–130
19. Escartin C, Galea E, Lakatos A, O'Callaghan JP, Petzold GC, Serrano-Pozo A, Steinhäuser C, Volterra A, Carmignoto G, Agarwal A et al (2021) Reactive astrocyte nomenclature, definitions, and future directions. *Nat Neurosci* 24:312–325
20. Demirs JT, Yang J, Crowley MA, Twarog M, Delgado O, Qiu Y, Poor S, Rice DS, Dryja TP, Anderson K, Liao SM (2021) Differential and altered spatial distribution of complement expression in age-related macular degeneration. *Invest Ophthalmol Vis Sci* 62:26
21. Cattell RB (1966) The scree test for the number of factors. *Multivar Behav Res* 1:245–276
22. Yeomans KA, Golder PA (1982) The guttmann-kaiser criterion as a predictor of the number of common factors. *J Royal Statistical Soc Series D (The Statistician)* 31:221–229
23. Kaiser HF (1958) The varimax criterion for analytic rotation in factor analysis. *Psychometrika* 23:187–200
24. Caliński T, Harabasz J (1974) A dendrite method for cluster analysis. *Commun Stat* 3:1–27
25. Tatham AJ, Weinreb RN, Zangwill LM, Liebmann JM, Girkin CA, Medeiros FA (2013) The relationship between cup-to-disc ratio and estimated number of retinal ganglion cells. *Investig Ophthalmology Vis Sci* 54:3205
26. Quigley HA, Green WR (2020) The histology of human glaucoma cupping and optic nerve damage: clinicopathologic correlation in 21 eyes. *Ophthalmology* 127:S45–S69
27. Moghimi S, Zangwill LM, Manalastas PIC, Suh MH, Penteado RC, Hou H, Hasenstab K, Ghahari E, Bowd C, Weinreb RN (2019) Association between lamina cribrosa defects and progressive retinal nerve fiber layer loss in glaucoma. *JAMA Ophthalmology* 137:425
28. Quigley HA, Green WR (1979) The histology of human glaucoma cupping and optic nerve damage: clinicopathologic correlation in 21 eyes. *Ophthalmology* 86:1803–1827
29. García-Bermúdez MY, Freude KK, Mouhammad ZA, van Wijngaarden P, Martin KK, Kolko M (2021) Glial cells in glaucoma: friends, foes, and potential therapeutic targets. *Front Neurol* 12:624983
30. Salkar A, Wall RV, Basavarajappa D, Chitranshi N, Parilla GE, Mirzaei M, Yan P, Graham S, You Y (2024) Glial cell activation and immune responses in glaucoma: a systematic review of human postmortem studies of the retina and optic nerve. *Aging disease*. 15(5):1069
31. Monavarfeshani A, Yan W, Pappas C, Odenigbo KA, He Z, Segrè AV, Zyl TV, Hageman GS, Sanes JR (2023) Transcriptomic analysis of the ocular posterior segment completes a cell atlas of the human eye. *Cold Spring Harb Lab* 9:e144
32. Plaza-Zabala A, Sierra-Torre V, Sierra A (2017) Autophagy and microglia: novel partners in neurodegeneration and aging. *Int J Mol Sci* 18:598
33. Ramírez AI, De Hoz R, Salobar-García E, Salazar JJ, Rojas B, Ajoy D, López-Cuenca I, Rojas P, Triviño A, Ramírez JM (2017) The role of microglia in retinal neurodegeneration: alzheimer's disease, parkinson, and glaucoma. *Front Ag Neurosci* 9:214
34. Wang K, Peng B, Lin B (2014) Fractalkine receptor regulates microglial neurotoxicity in an experimental mouse glaucoma model. *Glia* 62:1943–1954
35. Ferreira-Silva J, Aires ID, Boia R, Ambrósio AF, Santiago AR (2020) Activation of adenosine A3 receptor inhibits microglia reactivity elicited by elevated pressure. *Int J Mol Sci* 21:7218
36. Aires ID, Boia R, Rodrigues-Neves AC, Madeira MH, Marques C, Ambrósio AF, Santiago AR (2019) Blockade of microglial adenosine A_{2A} receptor suppresses elevated pressure-induced inflammation, oxidative stress, and cell death in retinal cells. *Glia* 67:896–914
37. Chidlow G, Daymon M, Wood JP, Casson RJ (2011) Localization of a wide-ranging panel of antigens in the rat retina by immunohistochemistry: comparison of Davidson's solution and formalin as fixatives. *J Histochem Cytochem* 59:884–898
38. Han X, Steven K, Qassim A, Marshall HN, Bean C, Tremere M, An J, Siggs OM, Gharahkhani P, Craig JE et al (2021) Automated AI labeling of optic nerve head enables insights into cross-ancestry glaucoma risk and genetic discovery in >280,000 images from UKB and CLSA. *Am J Hum Genet* 108:1204–1216

Publisher's Note

Springer Nature remains neutral with regard to jurisdictional claims in published maps and institutional affiliations.